PROBLEMY MECHATRONIKI
UZBROJENIE, LOTNICTWO, INŻYNIERIA BEZPIECZEŃSTWA

ISSN 2081-5891

7, 4 (26), 2016, 33-66

PROBLEMS IN MECHATRONICS
ARMAMENT, AVIATION, SAFETY ENGINEERING

Determination of the Firing Pin Critical Velocity and the Critical Power in the Percussive Initiation of Primer Caps

Andrzej FARYŃSKI*, Andrzej DŁUGOŁĘCKI, Jarosław DĘBIŃSKI, Łukasz SŁONKIEWICZ

Air Force Institute of Technology
6 Księcia Bolesława Street, 01-494 Warsaw, Poland
* *Corresponding author's e-mail address: andrzej.farynski@itwl.pl*

Received by the editorial staff on 5 May 2014.
The reviewed and verified version was received on 7 April 2016.

DOI 10.5604/01.3001.0009.5019

Abstract: This work involved testing of the probability of initiating a KWM-3 type of primer cap as a function of the firing pin velocity upon impact. The tested firing pin was accelerated to the required velocity by a falling mass. The measurements under this work were made with a measurement system and methodologies developed at Air Force Institute of Technology (AFIT) in Warsaw (Poland). The percussive pulse velocity and power was altered by modifying the percussive mass to keep the initiating pulse energy constant at two levels: E_{we} = 272 mJ and 343 mJ. The firing pin velocity values estimated by experimental data to bring a 50% probability of percussive primer cap initiation were within the interval $v_{i50\%}$ = 0.34÷0.51 m/s. It was found that the mean primer cap ignition delay rose from approx. 0.7 ms at a percussion velocity of 1.5 m/s to 6 ms at 0.17 m/s. The experimental data suggest the values of $E_{we} \times v_{i50\%} \approx 0.136$. A simplified model was proposed for the deformation of the primer cap base and compressed pyrotechnical mixture shape.

This work has been compiled from a paper presented during the 10th International Armament Conference on "Scientific Aspects of Armament and Safety Technology", Ryn, Poland, September 15–18, 2014.

The model served to determine the approximate time trend for the penetration of the primer cap by the firing pin, including velocity, power and emitted energy, by assuming a complete energy transfer from the percussive mass to the primer cap.

The average time initiating pulse power calculated from the model at the $v_{i50\%}$ was P_{avg} = 120÷180 W, whereas the maximum initiating pulse power was P_{max} = 170÷250 W. The calculated time values for firing pin penetration were very close to the aforementioned primer cap ignition delays at the respective velocity and percussive mass values. This indirectly indicates nearly complete energy transmission from the percussive masses to the primer caps. A location was identified within the compressed pyrotechnical mixture shape volume which could form the hot spot for initiation of the explosive reaction. Based on the calculation results using the simplified model, and assuming that the speed energy transfer to – and diffusive heat flux output from – the explosive reaction initiation hot spot were equivalent, the expression of $E_{we} \times v_{i50\%}$ derived from the result was approx. 0.18. This means that the two critical parameters of primer cap initiation: velocity, which can be identified with $v_{i50\%}$ (and the respective power) and $E_{we50\%}$, i.e. the energy threshold below which the probability of primer cap initiation is less than 0.5, are interrelated. Aside from the initiation mechanism proposed and applied to calculate the firing pin critical velocity, this work discusses several other initiation mechanisms, all of which were ruled out during the testing process.

Keywords: mechanics, percussive primer cap initiation, critical power, time delay, ignition probability

1. INTRODUCTION

This work tested the conditions required to initiate ignition of a KWM-3 primer cap, a product used to trigger the cartridges (such as PK-16) applied in aircraft ejection seats.

In the tests discussed here, the KWM-3 primer cap was percussively initiated by a firing pin with specific kinetic energy E_{we}. This kinetic energy was delivered to a firing pin of known mass, m_U (being a percussion striker) which fell by force of gravity from a known height h ($E_{we} = m_U \cdot g \cdot h$, where g = gravitational acceleration). The equipment used for these tests was designed to cause plastic deformation of the primer cap only during the stroke, while the contact during the elastic impact of the percussive mass with the firing pin was assumed to be long enough to initiate the primer cap.

The testing of initiating conditions are routine in the operation of pyrotechnical systems and consists of the verification of the primer cap initiation probability $p(E_{we})$ at two energy levels predefined by the primer cap manufacturer: E_{weD}, where the desired probability is $p(E_{weD}) = 0$, and $E_{weG} > E_{weD}$, where the desired probability is $p(E_{weG}) \approx 1$. The more complex tests for determination of E_{weD} and E_{weG}, consist of the verification of $p(E_{we})$ at several (at least) gradually increasing values of E_{we}.

The distribution function $p(E_{we})$ built into the process enabled determination of the median $E_{we50\%}$ and the standard deviation σ_E, where $E_{weD} = E_{we50\%} - n_D \cdot \sigma_E$, $E_{weG} = E_{we50\%} + n_G \cdot \sigma_E$; and n_D, $n_G < 10$.

For the primer caps tested here: $E_{we50\%} \approx 170$ mJ, $\sigma_E \approx 60$ mJ [1], although the values could vary between individual production runs of the primer caps.
During the tests listed above, made at m_U = const, E_{we} changed naturally with its mean input power, P_{we}: a change of h changed the percussion striker impact velocity $v_U = (2 \cdot g \cdot h)^{1/2}$ related to the input power. For firing pin masses much less than m_U, $v_{igl} \approx v_U$ can be assumed.

This brought up a question needing an answer: should the routine testing of primer caps focus only on compliance with the energy condition ($E_{we} \geq E_{weG}$) and disregard the conditions relative to the energy transmission power?

This work was an attempt to answer this question. The primary objective here was to demonstrate a relationship between primer cap initiation probability and the firing pin initial velocity v_{igl} at a constant energy input E_{we}. It was demonstrated that the dependence on v_{igl} under these conditions was equivalent to the dependence on the mean energy input power of the firing pin. Velocity v_{igl} proved much more convenient in use than P_{we}. Its value can be easily determined during experimentation; hence this work generally replaced P_{we} with v_{igl}. Given that if $v_{igl} \rightarrow 0$ then $p(v_{igl}) \rightarrow 0$, an assumption was made that for a given E_{we} a **firing pin critical velocity value** existed, $v_{igl(kryt)}$, below which primer cap initiation (ignition) would not be possible; hence the need to reach $p(E_{we}) \approx 1$, $v_{igl} > v_{igl(kryt)}$. This critical value, not unlike E_{weD} and E_{weG}, would be specific for a **specific type** of primer cap.

An attempt was then made to achieve a theoretical determination of $v_{igl(kryt)}$. Simplified models were assumed for: deformation of the primer cap metallic base dented by the firing pin, and the deformation (crushing) of the pyrotechnical mixture (PM) shape, contained in the primer cap, by deformation of the base. The calculations based on these models were intended to depict the kinematics of the primer cap penetration by the firing pin and the concomitant forces, as well as the time trend of energy output from the deformed primer cap base and (separately) from the deformed PM. A part of the deformed PM energy output was spent on initiating the PM reaction. The $v_{igl(kryt)}$ was evaluated using a simplified model of heat output, which was partially based on the aforementioned calculation results.

2. EXPERIMENTAL DETERMINATION OF FIRING PIN CRITICAL VELOCITY

The tests to determine $v_{igl(kryt)}$ were made with a weight drop stand [1] and two batches of primer caps from two different production runs, conventionally labelled "Lot A" and "Lot B". Percussion strikers of different mass m_U were dropped on a firing pin with mass m_{igl} = 12.25 g.

Due to technical constraints, v_{igl} (equated with v_U, on the conditions presented below) was modified within a technically permitted range. E_{we} was determined so as to produce the initiation probability $p(v_{igl}) > 0.9$ at the lowest of the tested masses.

Lot A was tested at m_U = 307 g, 774 g and 2376 g, which, given the available energy $E_{we} = m_U v_{igl}^2 / 2 = 272 \pm 2$ mJ = const, provided the initial velocity v_{igl} = 1.33, 0.84, and 0.48 m/s, respectively.

A group N_G = 30 primer caps was used for each of the velocity values. The ignition probability was determined as $p(v_{igl}) = N_Z / N_G$, with N_Z being the successfully initiated primer caps in the test group. The determination error of $p(v_{igl})$ was estimated at $\Delta p(v_{igl}) \approx 1 / N_G \approx 3.3\%$.

The experimental test results are shown in Table 1 and Fig. 1, where the diamonds show the experimentally determined primer cap initiation probability $p(v_{igl})$.

Table 1

	Lot A			Lot B			
v_{igl}, m/s	1.329	0.837	0.478	1.5	0.942	0.537	0.172
N_Z / N_G	28 / 30	24 / 30	15 / 30	28 / 30	25 / 30	28 / 40	17 / 60
$p(v_{igl})$	0.933	0.8	0.5	0.933	0.833	0.7	0.283

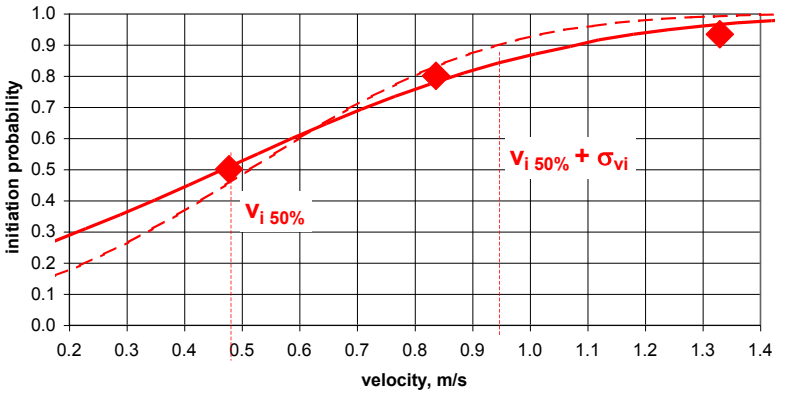

Fig. 1. Initiation probability distribution function vs. firing pin velocity at E_{we} = 272 mJ = const for the Lot A primer caps; the highlighted $v_{i50\%}$ and $v_{i50\%} + \sigma_{vi}$ apply to the normal distribution of 3 experimental points; the dashed curve is a ND function based on the same 3 points with the addition of a point at: (0,0)

The solid curve in Fig. 1 is the normal distribution (ND) function approximating to the set of 3 experimental points (3P) in a manner explained in [1]. The dashed curve is the ND function approximating the same set with the addition of a point at (0,0); this appendix is justified since $v_{igl} = 0$ is equivalent to the lack of percussion and no initiation achieved ($p(v_{igl}) = 0$).

The ND was selected since no premises existed for choosing a different distribution form, and the ND was deemed to be **the most probable**. The 3P distribution function was approximated in parallel with several distribution types: an exponential distribution was used with a uniform distribution [1] to evaluate the error imposed by the assumed ND form. The determined v_{igl} value at $p(v_{igl}) = 0.5$ was $v_{i50\%} = 0.49$ m/s for the ND (the mean for the distributions: 3P and 3P with appended (0,0)) at a standard deviation $\sigma_{vi} = 0.41$ m/s; $v_{i50\%}$ and σ_{vi} for the uniform distribution were 0.39 m/s and 0.58 m/s, and respectively for the exponential distribution, 0.41 m/s and 0.081 m/s.

Lot B was tested in a similar way, where m_U = 307 g, 774 g, 2376 g and 23.3 kg, and given E_{we} = 343±2 mJ = const, and the resulting velocity values were, respectively, v_{igl} = 1.50, 0.94, 0.54, and 0.17 m/s.

The primer cap groups initiated at these velocity values included 30, 30, 40 and 60 caps, respectively. Here, the determination error for the initiation probability at v_{igl} was, respectively, $\Delta p(v_{igl}) \approx$ 3.3%, 2.5% and 1.7%. The estimated error for the presumed percussion striker energy retention ranged from 1.9% at 1.50 m/s to 15% at 0.17 m/s.

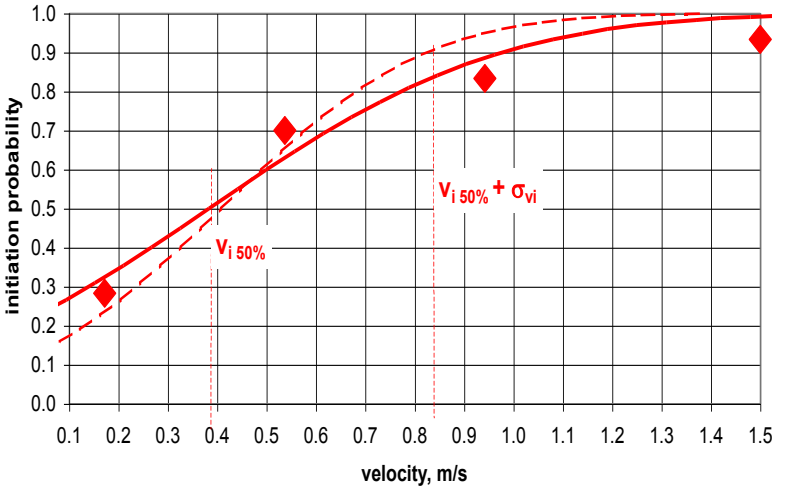

Fig. 2. Initiation probability distribution function vs. firing pin velocity at E_{we} = 343 mJ = const for the Lot B primer caps; the highlighted $v_{i50\%}$ and $v_{i50\%} + \sigma_{vi}$ apply to a normal distribution of 4 experimental points; the dashed curve is a ND function based on the same 4 points with the addition of a point at: (0,0)

The test results are also shown in Table 1 and in Fig. 2 in the same way as in Fig. 1; however, this time the approximations were made for a set of four experimental points, 4P, and for 4P including point (0,0).

In this case, $v_{i50\%}$ = 0.40 m/s for the ND (a mean value for the distributions approximated with sets 4P and 4P with appended point (0,0)) at a standard deviation σ_{vi} = 0.39 m/s; the values of $v_{i50\%}$ and σ_{vi} with the uniform distribution were 0.38 m/s and 0.63 m/s, and, respectively for the exponential distribution, 0.34 m/s and 0.068 m/s. The latter two values applied to the approximation with 4P only.

The assumed firing pin initial velocity v_{igl} was equated with the percussion striker velocity v_U, determined directly from its drop height. Given the mass of the firing pin and of the percussion strikers used for testing, v_{igl} was slightly lower than v_U. The related error $|\Delta v_{igl} / v_{igl}| = m_{igl} / m_U$, as calculated from the law of conservation of momentum (where a part of the energy of a completely non-elastic impact is consumed by the deformation related to the combination of masses), was 3.99%, 1.58%, 0.52% and 0.053% for, respectively, m_U = 307 g, 774 g, 2376 g and 23.3 kg; in the last mass instance, the determination error of m_U was ~0.1%. It is evident that the error from the assumption that $v_{igl} \approx v_U$ was equal to or smaller than all other errors.

The issue of the correspondence of v_{igl} with the energy transfer from the percussion striker to the firing pin was investigated further.

Note that the primer cap initiation probability was $p_{init} \approx p(E_{we} \geq E_{prog}) \times p(v_{igl} \geq v_{igl(kryt)})$, with E_{prog} being the initiation energy threshold, and where $p\ (E_{we} \geq E_{prog}) \sim const_1 \times E_{we} / E_{prog}$, $p(v_{igl} \geq v_{igl(kryt)}) \sim const_2 \times v_{igl} / v_{igl(kryt)}$ ($const_1$, $const_2$ being the normalization constants). Hence the condition $p(v_{i50\%}) \approx E_{we} \times v_{i50\%} \times const_1 \times const_2 / v_{igl(kryt)} / E_{prog} \approx 0.5$ and the aforementioned information mean that $E_{we} \times v_{i50\%} \approx$ const, see Table 2:

$$v_{i50\%} \approx 0.136 / E_{we} \tag{1}$$

Table 2

E_{we}, mJ	$v_{i\ 50\%}$, m/s	$E_{we} \times v_{i\ 50\%}$, J × m/s
273	0.49	0.1338
343	0.40	0.1372

Note that the relationship (1) is specific only to type KWM-3 primer caps; here the constant was determined from a relatively limited quantity of data, and further investigation is required in order to refine it. The constant may vary for other primer cap types.

The other tests mentioned in the introduction involved the simultaneous adjustments of E_{we} and v_{igl} (by adjusting the drop height) to determine $E_{we50\%}$ for the primer caps from different batches. The values resulting from these tests and their products are shown in Table 3.

Table 3

$E_{we50\%}$,mJ	v_{igl} , m/s	$E_{we50\%} \times v_{igl}$, J × m/s
191	0.847	0.1618
163	1.03	0.1697
177	1.07	0.1901

The products of $E_{we50\%} \times v_{igl}$ from Table 3 and $E_{we} \times v_{i50\%}$ from Table 2 are approximate in value, which may suggest a **pair of coupled** critical values.

An investigation into the relationship of $v_{i50\%}$ with $v_{igl(kryt)}$ required consideration of the process of penetrating the primer cap by the firing pin. The process was analysed with the following deformation model of primer cap base and PM shape.

3. PENETRATION MODEL OF THE PRIMER CAP BY THE FIRING PIN

3.1. Primer cap metal base deformation

Figure 3 shows a view of the bases of the initiated primer caps as deformed by the firing pin. The form of indentation can be approximated to the ball-shaped tip of the firing pin. The model assumed indentation by the firing pin as shown by the cross-section of a primer cap in Fig. 4. The PM shape rests against a brass anvil, covered with the brass base of the primer cap. The PM shape is compressed between the anvil and the primer cap base by the pressure from the firing pin. Here the anvil is stationary. The firing pin tip radius is r_i. The impression of the firing pin to a depth x_i ($v = dx_i/dt$ – the firing pin velocity, t – time) corresponds to the indentation radius:

$$r_w = (r_i^{\,2} - (r_i - x_i)^2)^{1/2} \tag{2}$$

The anvil has a radius r_K on which the PM shape rests and is connected to the primer cap by three brackets, the total cross-sectional area of which is equal to or higher than the anvil surface area. The primer cap base metal has yield strength R_m and shear strength R_T; according to a hypothesis by M.T. Huber, $R_T \approx 0.6 \cdot R_m$ [2]. The axial force of the deformed base resistance to the firing pin was determined as follows.

Fig. 3. Indentation marks from the firing pin on the primer cap bases of a cartridge

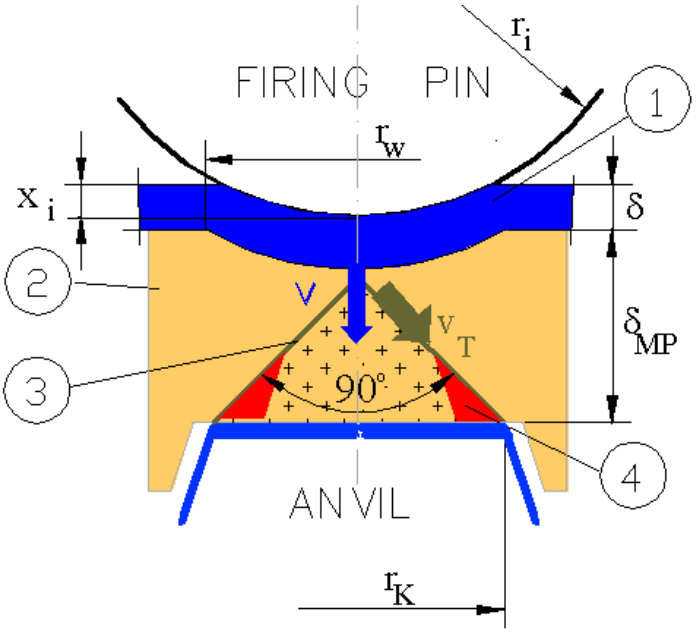

Fig. 4. Diagram of PM crushing by the firing pin: 1 – primer cap base; 2 – PM shape; 3 – tapered (SW) surfaces Σ of PM shearing/slip; 4 – probable location of the peak heat output and chemical reaction initiation; $\delta_{MP} \approx 0.65$ mm – original thickness of the PM section exposed to crushing; v, v_T – velocity of the firing pin and the PM slip

It was assumed that the indentation boundary ($r = r_w$) on a primer cap base, with thickness of δ, is where the base is subject to plastic shearing as a function of indentation depth x_i at a force [3]:

$$F_T(x_i) \approx R_T \cdot S_{D,}$$

with:
$$S_D = 2 \cdot \pi \cdot \delta \cdot r_w \qquad (3)$$

as the shearing surface; hence:

$$F_T(x_i) \approx 2 \cdot \pi \cdot \delta \cdot R_T \cdot (r_i^{\,2} - (r_i - x_i)^2)^{1/2}$$

combined with the plastic tension of the primer cap base with a force that features an axial component, $F_R(x_i) = F_{RS}(x_i) \cdot \sin \alpha$, with α as the angle between the spherical indentation surface tangent and the primer cap base surface: $\sin \alpha = (r_i^2 - (r_i - x_i)^2)^{1/2} / r_i$. $F_{RS}(x_i)$ is the force tangential to the spherical indentation surface: $F_{RS}(x_i) = R_m \cdot S_D$. An assumption was made that the surface S_D may be equal to the shearing surface (3) or its projection to a normal to $F_{RS}(x_i)$: $S_D \cdot \cos \alpha = 2 \cdot \pi \cdot \delta \cdot (r_i^2 - (r_i - x_i)^2)^{1/2} \cdot (r_i - x_i) / r_i$.

Hence the axial component of force originating from the tension action on the primer cap base can be expressed as:

$$F_R(x_i) \approx 2 \cdot \pi \cdot \delta \cdot R_m \cdot (r_i^2 - (r_i - x_i)^2) / r_i$$

or

$$F_R(x_i) \approx 2 \cdot \pi \cdot \delta \cdot R_m \cdot (r_i^2 - (r_i - x_i)^2) \cdot (r_i - x_i) / r_i^2$$

Given these assumptions, the overall force of primer cap base deformation was resolved as follows in further calculations:

$$F_{TR}(x_i) = F_T(x_i) \approx 1.2 \cdot \pi \cdot \delta \cdot R_m \cdot (r_i^2 - (r_i - x_i)^2)^{1/2} \quad (4)$$

or

$$F_{TR}(x_i) = F_T(x_i) + F_R(x_i) \approx 2 \cdot \pi \cdot \delta \cdot R_m \cdot [0.6 \cdot (r_i^2 - (r_i - x_i)^2)^{1/2} + (r_i^2 - (r_i - x_i)^2) / r_i] \quad (5)$$

or

$$F_{TR}(x_i) = F_T(x_i) + F_R(x_i) \approx 2 \cdot \pi \cdot \delta \cdot R_m \cdot [0.6 \cdot (r_i^2 - (r_i - x_i)^2)^{1/2} + (r_i^2 - (r_i - x_i)^2) \cdot (r_i - x_i) / r_i^2] \quad (6)$$

3.2. The proposed model of PM deformation during indentation with the firing pin

The effects that occur within the PM subject to compression and which lead to initiation of the mixture are complex enough to require a simplified model for any estimation related to them. A model of this system needs to be designed with consideration of the specific primer cap type design. The model proposed below applies to KMW-3 type primer caps.

In the tested KMW-3 primer caps, an PM shape with a mass m_{PM} = 51 mg is pressed into a brass cup with a diameter of approx. 3.4 mm and a wall thickness of approx. 0.4 mm [4], with the open end on the anvil side (Fig. 4).

Given the high pressure applied to manufacture the PM shape, it can be assumed to be a homogeneous, brittle medium with the mechanical and thermal characteristics approximate to those of water ice or ceramic, e.g. bricks. During the intended action time, the PM shape is subject to axial compression between the firing pin and the anvil.

The flat-wise axial compression of this homogeneous medium with restricted radial dimensions according to equation [2] results in an input of shearing stresses. The shearing stresses reach their maximum values at the tapered surfaces that rest on axially symmetric compressing surfaces. The compressing surfaces form the bases for the tapered surfaces. The angle between the generating lines of the tapers and the bases is approx. 45°. When the shear strength limit R_{PM} is exceeded, the PM on the outside of the tapers is pushed in a radial direction and slides on the tapered surfaces at velocity v_T.

During the intended action time of the primer cap, the only time-invariable (assumed) is the anvil surface area with the radius r_K; the surface area with the radius r_w is formed by the indentation from the firing pin and grows in time; hence the shearing cylinder based on the latter surface moves to the inside of the PM medium and on the outside of the axis in an undetermined manner. The PM shape is laterally supported by the primer cap walls, so the actual state of stress and displacement will vary from the ideal model presented above; however, for the sake of estimation, **the following simplifications were assumed**:

- The firing pin indents the primer cap by moving along its centreline (axis) with a transient velocity v, $v(t = 0) = v_{igl}$.
- The PM shearing effect occurs on the surface of a cylinder with radius r_w and height δ_{MP} (as in the deformation of the primer cap base), whereas the shearing and slip occur on the surface Σ of the stationary PM internal cone (SW) with an apical of 90° and height r_K; the cone rests on the anvil surface (as shown dotted in Fig. 4); this is the difference between this model and that in the work [3]. An auxiliary coordinate x was assumed within SW (see Section 3.2) and with an origin ($x = 0$) at the SW apex. The x coordinate is aligned with the SW axis and has a positive sense towards the SW base ($x = r_K$).
- From $t = 0$, the PM section impressed by the firing pin is displaced at v towards the firing pin axis within a cylinder with a radius r_w and towards the SW apex. The PM section behaves like an incompressible liquid with a constant radial velocity distribution. The said PM "liquid" (LPM) was assumed to flow around the SW at a velocity at the SW surface, expressed as follows:

$$v_{T1} = 2^{1/2}\, v \text{ with } x < r_w,\ r_w \le r_K \tag{7a}$$

$$v_{T1} = 2^{1/2}\, v \cdot r_w / r_K \text{ with } x = r_K \tag{7b}$$

and the velocity exhibits a linear change from (7a) to (7b):

$$\underline{v}_{T1}(x) = 2^{1/2}\, v \cdot (r_w / r_K) \cdot (1 - (x - r_K) / r_w),\ r_w \le x \le r_K \tag{7c}$$

or

$$\underline{v}_{T1}(x) = 2^{1/2}\, v \text{ with } 0 \le x \le r_K,\ r_w > r_K \tag{7d}$$

The friction of the LPM on the SW surface (i.e. shearing) results in stress R_{PM}. The equivalent force of axial resistance F_{1PMi} of the process against the firing pin was determined as follows.

The SW lateral surface area is $S_{con} = 2^{1/2}\, \pi \cdot r_K^2$, and its element at a distance x is $dS_{con}(x) \approx 2^{3/2}\, \pi \cdot x \cdot dx$. The elementary work of axial displacement is described by (7a) and (7c):

$$dW = F_{1PMi} \cdot v \cdot dt \equiv {}_0\int^{rK} R_{PM} \cdot dS_{con}(x) \cdot v_{T1}(x) \cdot dt =$$
$$= {}_0\int^{rw} R_{PM} \cdot dS_{con}(x) \cdot 2^{1/2} \cdot v \cdot dt +$$
$$+ {}_{rw}\int^{rK} R_{PM} \cdot dS_{con}(x) \cdot 2^{1/2} \cdot v \cdot (r_w / r_K) \cdot (1 - (x - r_K) / r_w) \cdot dt$$

hence:

$$F_{1PMi} = 2\cdot\pi\cdot R_{PM}\cdot r_K^2\cdot\{(r_w/r_K)^2 + (r_w/r_K)\cdot(1 - r_w/r_K)\cdot[(1 + r_w/r_K)^2 + 2\, r_w/r_K] / 3\}$$

with $r_w \le r_K$ (8)

The rapid surge in the force was a computational inconvenience and eliminated as follows: for $r_w > r_K$ was assumed to change linearly as a function of x_i between $F_{1PMi} = 2\ R_{PM} \cdot \pi \cdot r_K^2$ and $F_{2PMi}(x_{i0})$ (see below).

- An assumption was made that from $t = t_0$, which corresponded to:

$$x_i(t_0) = \delta_{PM} - r_K = x_{i0} \tag{9}$$

and at which the indented primer cap base makes contact with the SW apex, the base begins to shear the SW apex, and the sheared apex material flows since then out of the axis, being added to the kinematically determined LPM flux that flows around the further part of SW and increases the flux axial velocity by v_{dod},:

$$\pi \cdot (x_i - x_{i0})^2 \cdot v \cdot \mathrm{d}t \approx \pi \cdot v_{dod}\cdot(r_w^2 - (x_i - x_{i0})^2)\ \mathrm{d}t$$

dt – time differential,

$$v_{dod} = v \cdot (x_i - x_{i0})^2 / (r_w^2 - (x_i - x_{i0})^2)$$

hence the total axial velocity is: $v + v_{dod} = v\cdot r_w^2 / (r_w^2 - (x_i - x_{i0})^2)$
whereas the tangential velocity is:

$$v_{T2}^{\ *} = 2^{1/2}\, v\cdot r_w^2 / (r_w^2 - (x_i - x_{i0})^2) \tag{10a}$$

Given that the LPM cross-section area is constant within a cylinder with the radius r_w, the formula is transformed into the following expression at the SW base surface:

$$v_{T2} = 2^{1/2}\, v \cdot r_w^2 / (r_w^2 - r_K^2) \tag{10b}$$

For the sake of simplification of the calculation, it was assumed that, at any given moment, the LPM flux along the SW generating line as a function of the x coordinate exhibits a linear change from the value given in (10a) to the value from (10b), which can be expressed with this formula:

$$\underline{v}_{T2}(x) = 2^{1/2}\, v\cdot(r_w^2 / (r_w^2 - r_K^2)) \cdot (1 - r_K \cdot a_1 + a_1 \cdot x) \tag{10c}$$

$$a_1 = (r_K + (x_i - x_{i0})) / (r_w^2 - (x_i - x_{i0})^2)$$

$$x_i - x_{i0} \le x \le r_K$$

For an SW cross-section perpendicular to the axis and at the height $x_i - x_{i0}$, and from which the PM is expelled outwards at time t, a linear displacement velocity is assumed from 0 at $r = 0$ to v_{dod} at $r = x_i - x_{i0}$:

$$v_r(r) = v \cdot (x_i - x_{i0}) \cdot r / (r_w^2 - (x_i - x_{i0})^2)$$

Similar to $t \le t_0$, an expression was derived for the equivalent force of axial resistance F_{2PMi}:

$$dW = F_{2PMi} \cdot v \cdot dt \equiv \int_{xi-xi0}^{rK} R_{PM} \cdot dS_{con}(x) \cdot \underline{v}_{T2}(x) \cdot dt + \\ + \int_{0}^{xi-xi0} R_{PM} \cdot 2 \cdot \pi \cdot r \cdot dr \cdot v_r \cdot dt$$

and, when transformed, it becomes:

$$F_{2PMi} = 2 \cdot \pi \cdot R_{PM} \cdot r_K^2 \cdot \{((r_w / r_K)^2 / ((r_w / r_K)^2 - 1)) \cdot \\ \cdot (1 - ((x_i - x_{i0}) / r_K)^2) \cdot [3 \cdot (r_w / r_K)^2 - ((x_i - x_{i0}) / r_K)^2 - 1 - (x_i - x_{i0}) / r_K] + (11) \\ + ((x_i - x_{i0}) / r_K)^4\} / ((r_w / r_K)^2 - ((x_i - x_{i0}) / r_K)^2) / 3$$

It was noted that as long as the firing pin continues to indent the primer cap, the force F_{PMi}: $\{F_{1PMi}, F_{2PMi}\}$ occurs in parallel with the PM shearing force on the surface of the cylinder with the radius r_w, and by analogy to (4), this shearing force is:

$$F_{PMo}(x_i) \approx 2 \cdot \pi \cdot \delta_{PM} \cdot R_{PM} \cdot (r_i^2 - (r_i - x_i)^2)^{1/2} \qquad (12)$$

Figure 5 shows the progression of the forces determined in Sections 3.1 and 3.2 as a function of the firing pin penetration.

The primer cap base thickness for the calculations is δ = 0.4 mm, the crushed PM layer thickness is δ_{PM} = 0.65 mm, and the anvil radius is r_K = 0.5 mm [4], [3], R_{PM} = 14.7 MPa [3]. Denotation: FMPout – PM shearing force (12) over the radius r_w; FPMi – force at SW, with the successive formulas (8) and (11) for the respective intervals of x_i.

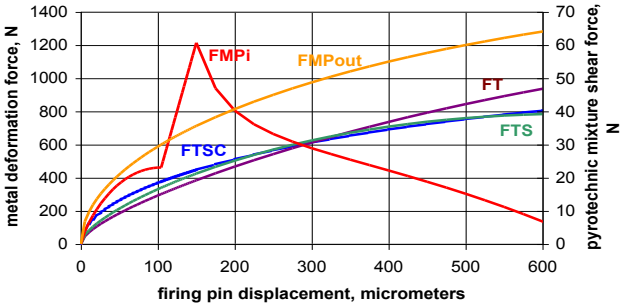

Fig. 5. Changes in individual components of the force of resistance vs. firing pin displacement; see text for details

The discontinuities of the derivative and the peak on the FMPi curve result from the lack of consistency between the slip velocities v_{T1} and v_{T2} of the model adopted in Section 3.2. FT is the primer cap base shearing force (4) at R_m = 500 MPa (which corresponds to R_T = 300 MPa of [3]); FTS is the force (5) of primer cap base deformation at R_m = 240 MPa; FTSC is the force (6) at R_m = 280 MPa.

The adopted R_m values in the calculation formulas applied here are within or approximate to the standard reference limits of 250-400 MPa [5] for brass; hence the trends of the forces (4), (5) and (6) are very much alike.

3.3. Simplified imaging of primer cap indentation with the firing pin

An approximation of the progress of the values describing the primer cap deformation during indentation with the firing pin with a ball tip radius of r_i = 1.25 mm was used to numerically integrate the equation for the firing pin movement (see the model in Fig. 4):

$$d^2x_i/dt^2 = -(F_{TR} + F_{PMo} + F_{PMi}) / m_U \qquad (13)$$

$$dx_i/dt = v$$

where the primer cap base and PM shearing forces F_{TR}, F_{PMo} and F_{PMi} are expressed as the formulas (4), (5), (6), (8), (11), (12) with initial conditions at $t = 0$: $x_i(0) = 0$, $dx_i/dt(0) = v(0) = v_{igl}$ and the percussion striker masses m_U used for the Lot B test caps (see Section 2, $\boldsymbol{E_{we}}$ **= 343 mJ**). The values δ, δ_{PM} and r_K were as assumed before. The instantaneous power was determined at $P(t) = F \cdot v$, where F denoted F_{TR}, F_{PMo} or F_{PMi}; the absorbed energy was determined at $E = \int F(t) \cdot v(t) dt$, where E denoted E_{Met}, E_{PMo} or E_{PMi}; E_{Met} was the energy output within the primer cap base; E_{PMo} was the energy output within the PM on a cylindrical surface with a growing r_w, and E_{PMi} was the energy output on the SW. A quasi-statistical approach was chosen due to the low velocities of penetration.

The calculation results are shown in Figs. 6 to 14. The curve plots in Figs. 6 to 11 show the progressions over time of the following values: v and x_i – firing pin velocity and penetration (displacement), FMet – primer cap base deformation force, FMPo – PM shearing force at the radius r_w; FPMi – force at the SW, and the following energy output powers: PMet – within the primer cap base, PMPo – at r_w within the PM, and PMPi – at the SW.

The curve plots in Figs. 12, 13 and 14 show the progressions over time of the energy output during the firing pin indentation: EMet – the energy output within the primer cap base, EMPo – the energy output within the MP at the growing r_w, and EMPi – the energy output at the SW.

Figures 6, 7 and 8 compare the effects of firing pin indentation at m_U = 307 g and the primer cap base deformation force expressed as (4), (5) and (6). The starting point for this comparison were the results produced with the assumption that the shearing effect was pure (see formula (4)) at R_m = 500 MPa.

The formulas (5) and (6) at this R_m value gave indentation time values too small when compared with the experimental data; the time length adjustment required R_m = 240 MPa in (5) and R_m = 280 MPa in (6).

(However R_m < 240 MPa in (5) and R_m < 280 MPa in (6) resulted in too rapid an evolution to the non-physical $x_i > \delta_{PM}$). The curves produced following these adjustments were very much alike in form and parameters; hence the analogical curves were prepared for other m_U values (Figs. 9, 10 and 11) and calculated only with (4) at R_m = 500 MPa. The peaks on the PMPi curves were derived from the FMPi peaks. The dynamics of firing pin indentation were defined by the material properties of the primer cap base.

Figs. 12 to 14 show a comparison of the energy output in the base, PM ring, formed by the indentation radius r_w, and SW of the primer cap during indentation by the firing pin; Fig. 12 complements Fig. 6 while Fig. 13 complements Fig. 11.

It is evident that for the model, the shape of curves EMet, EMPo and EMPi, and the final energy distribution between these locations at the firing pin stop for the given method of describing the primer cap base (Figs. 12 and 13), and the various types of base deformation (see formulas (4) and (6), and Figs. 12 and 14) do not particularly relate to m_U (i.e. v_{igl}). In each case, the final energy output EMPi to the SW (the internal cone of the PM) remained virtually identical.

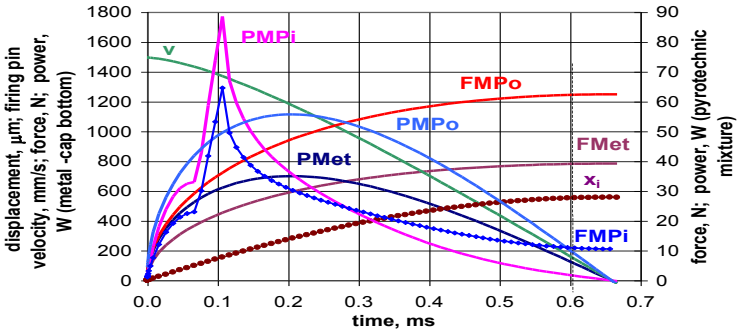

Fig. 6. The parameters of the quasi-static penetration of the KWM-3 primer cap base with the firing pin at E_{we} = 343 mJ and m_U = 307 g; the metal deformation force per formula (4); R_m = 500 MPa; see text for details

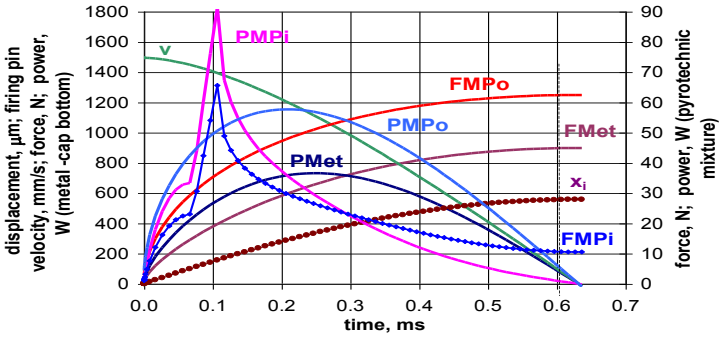

Fig. 7. The parameters of the quasi-static penetration of the KWM-3 primer cap base with the firing pin at E_{we} = 343 mJ and m_U = 307 g; the metal deformation force per formula (6); R_m = 280 MPa; see text for details

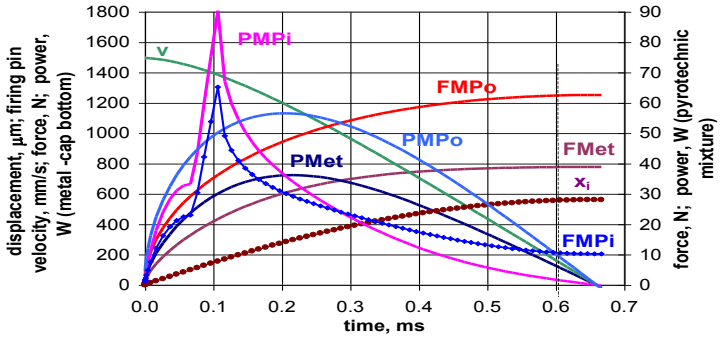

Fig. 8. The parameters of the quasi-static penetration of the KWM-3 primer cap base with the firing pin at E_{we} = 343 mJ and m_U = 307 g; the metal deformation force per formula (5); R_m = 240 MPa; see text for details

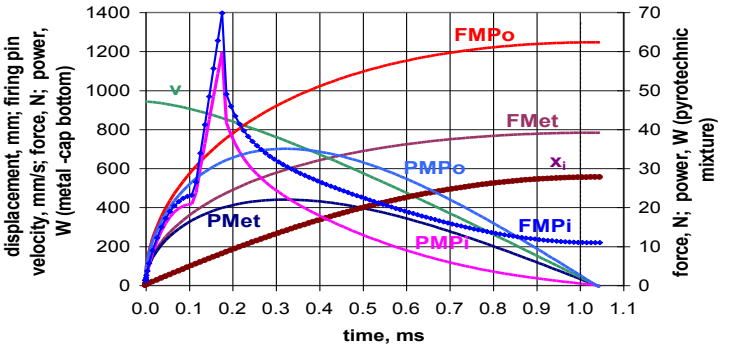

Fig. 9. The parameters of the quasi-static penetration of the KWM-3 primer cap base with the firing pin at E_{we} = 343 mJ and m_U = 774 g; see text for details

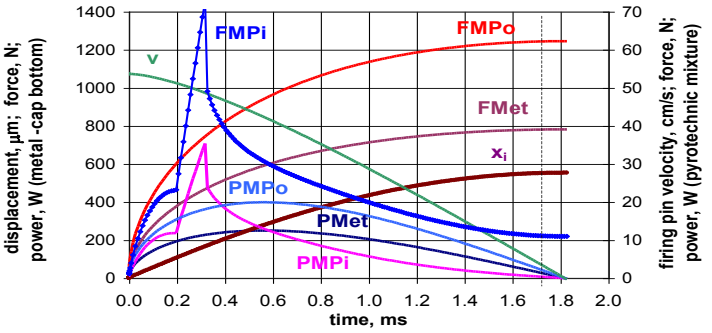

Fig. 10. The parameters of the quasi-static penetration of the KWM-3 primer cap base with the firing pin at E_{we} = 343 mJ and m_U = 2376 g; see text for details

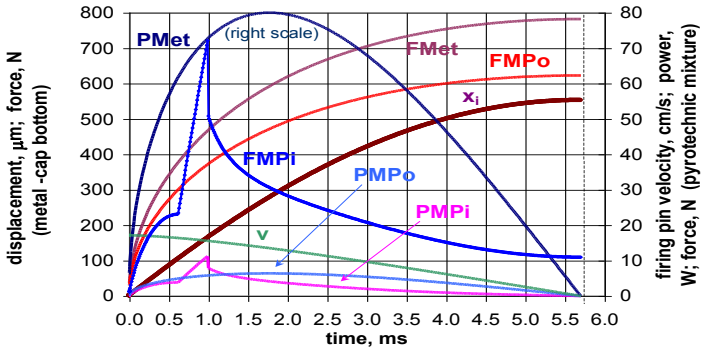

Fig. 11. The parameters of the quasi-static penetration of the KWM-3 primer cap base with the firing pin at E_{we} = 343 mJ and m_U = 23.3 kg; see text for details

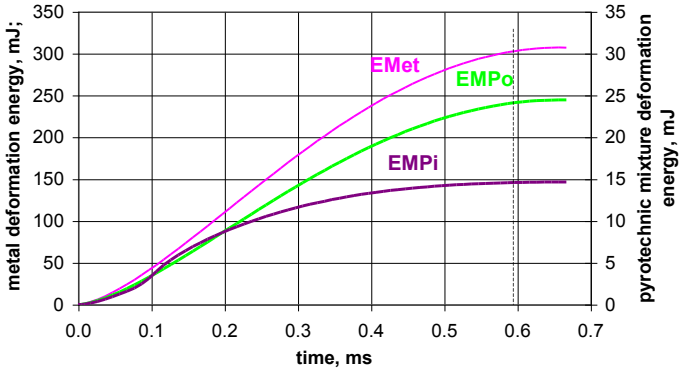

Fig. 12. Energy absorption (see text for details): m_U = 307 g, primer cap base shearing per formula (4), R_m = 500 MPa

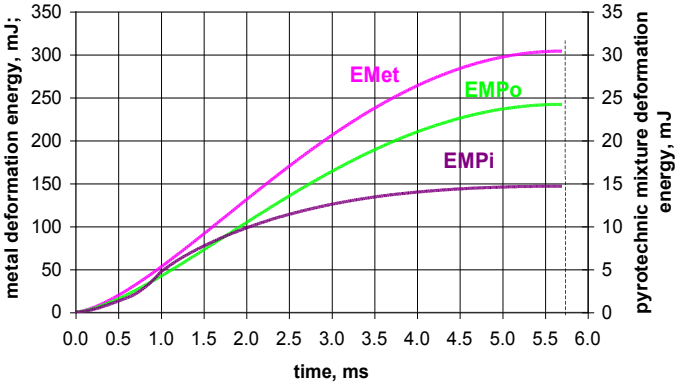

Fig. 13. Energy absorption (see text for details): m_U = 23.3 kg, primer cap base shearing according to formula (4), R_m = 500 MPa

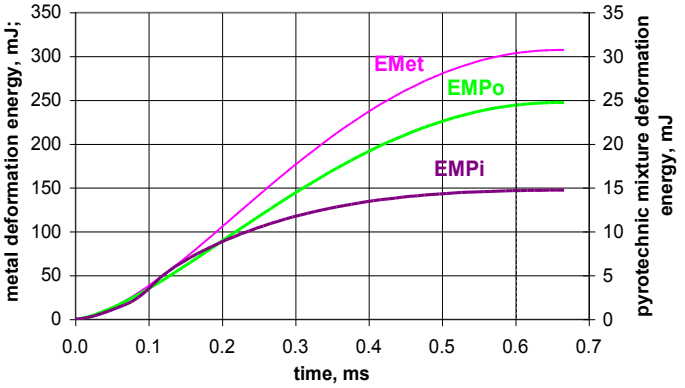

Fig. 14. Energy absorption (see text for details): m_U = 307 g, primer cap base deformation according to formula (6), R_m = 280 MPa

Figures 15 and 16 show the linear progressions of the maximum and mean deformation power of the primer cap base metal and PM as a function of v_{igl}. The charts confirm the equivalence of velocity v_{igl} and power P_{we} as the functions for investigation into primer cap initiation.

Table 4 lists the energy output values at various m_U and E_{we} = 343 mJ at τ_F near the end of the firing pin penetration (when x_i reaches d_z), which is the time when energy $E_{PMi} \approx 14.7$ mJ becomes an output on the PM internal cone. T, TS and TSC are the resulting variants of the calculation with formulas (4), (5) and (6), respectively.

Table 4

m_U, kg	formula	τ_F, ms	E_{Met}, mJ	E_{PMo}, mJ	E_{PMi}, mJ	d_z, mm
0.307	T	0.606	304	24.2	14.6	0.553
	TS	0.606	306	24.4	14.7	0.557
	TSC	0.606	304	24.5	14.7	0.557
0.774	T	1.016	304	24.2	14.7	0.553
	TS	0.966	304	24.3	14.7	0.554
	TSC	1.016	304	24.5	14.8	0.557
2.376	T	1.696	302	24.0	14.7	0.550
	TS	1.696	303	24.2	14.7	0.553
	TSC	1.716	302	24.3	14.7	0.555
23.3	T	5.65	304	24.2	14.7	0.553
	TS	5.47	304	24.3	14.7	0.554
	TSC	5.65	304	24.4	14.7	0.557

The firing pin penetration stop times τ_F can be compared to the measured time delay τ_{IGN} between the percussion striker impact on the firing pin (which is the firing pin penetration start) to the primer cap initiation time (i.e. when the flash occurs). The measurements made with the method explained in work [1] for each primer cap that was initiated during the aforementioned experiments (see Section 2) gave the mean τ_{IGN} values for the groups – see Table 5. The τ_{IGN} values are very approximate to τ_F.

Figure 15 also shows τ_{IGN} vs. v_{igl}. The measurement points (shown as red diamonds and triangles) on the chart were connected by a regression curve generated in an Excel spreadsheet. The regression curve equation *y*-value is the time delay, while the *x*-value is the firing pin initial velocity. It is evident that $\tau_{IGN} \times v_{igl} \approx 1$ was nearly ideal, which provides further evidence (see [3]) that the primer cap is initiated when the firing pin penetration reaches constant depth d_z. The mean calculated d_z value (see Table 4) was 0.554 mm.

Table 5

Lot A				
v_{igl}, m/s		0.478	0.837	1.33
τ_{IGN}, ms		1.790	0.899	0.551
Lot B				
v_{igl}, m/s	0.172	0.537	0.942	1.50
τ_{IGN}, ms	5.96	1.695	1.030	0.604

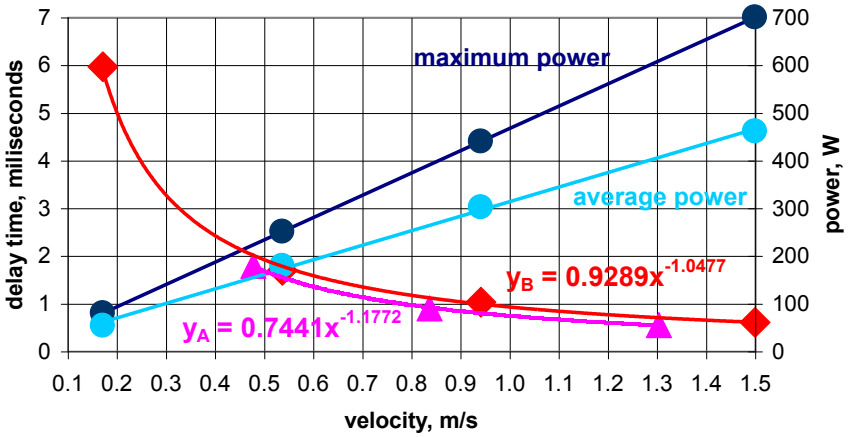

Fig. 15. The measured time delay (diamonds) to primer cap activation and the calculated metal deformation power as a function of the firing pin initial velocity v_{igl} at E_{we}= 343 mJ = const for the KWM-3 primer caps in Lot B; the triangles denote the time delay of Lot A (ref. regression curve equations: y_A, y_B – time delay of Lots A and B, respectively; x – firing pin initial velocity).

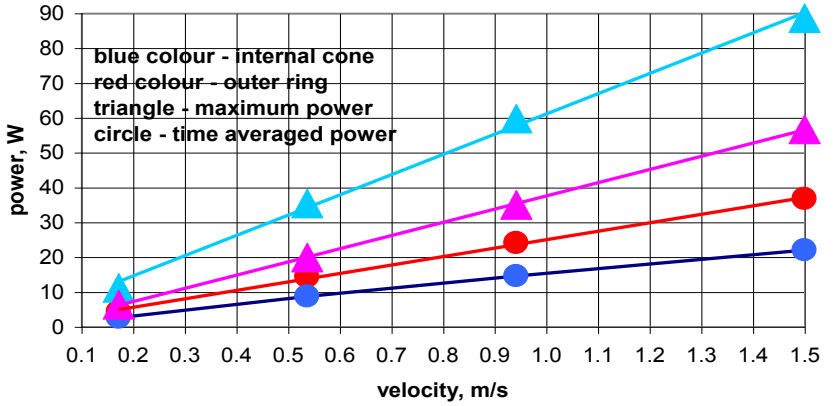

Fig. 16. Calculated MP deformation power vs. firing pin initial velocity v_{igl} at E_{we}= 343 mJ = const for the KWM-3 primer caps in Lot B; (internal cone – SW; outer ring – surface of a cylinder with $r = r_w$)

The calculations were made based on the assumption that the initial energy E_{we} was transferred effectively in full from the firing pin to the primer cap by non-elastic impact (i.e. with the firing pin resting on a plastic-deformable cap). The small differences between τ_F and τ_{IGN} show that the assumptions were very close to reality.

4. PENETRATION DEPTH IN THE HEAT DIFFUSION PROCESS

The diffusion of the heat input to the initiated PM shape of the primer cap is described with the following heat equation for a flat, mono-dimensional case (which was assumed to provide a sufficient description):

$$\partial^2 \Delta T/\partial x^2 - (\rho \cdot c_p / \lambda) \cdot \partial \Delta T/\partial t = 0 \tag{14}$$

with $\Delta T(x,t) = T(x,t) - T_{env}$; T, T_{env} – respectively: current medium temperature and initial (ambient) temperature, $\Delta T\ (x,0) = 0$, $\Delta T\ (\infty,t) = 0$; t – time, x – coordinate of the half space depth, ρ, c_p , λ – respectively: density, constant volume specific heat, and heat conductivity of the medium. Given the investigated problem, it is convenient to make further estimations with the solutions for two boundary condition cases.

4.1. Pre-set boundary power (heat flux): $P(t) = -\lambda \cdot \partial \Delta T/\partial x\ (0,t)$

The solution of equation (14) for a simple and special case of $P(t) = P_0 = \text{const}$ was derived numerically at the discrete time points $t = (k - 1)\ \Delta t$, $k = 1, 2, 3, \ldots$ and discrete spatial points of the medium, $x_n = (n - 1)\ \Delta x$, $n = 1, 2, \ldots, N$. The step Δx and N were chosen to have an x_N value high enough to simulate $x \to \infty$. By conversion of partial derivatives into finite differences, equation (14) gave an expression of the temperature gain values at the time space grid points:

$$\Delta T_{n,k+1} = \psi \cdot (\Delta T_{n+1,k} + \Delta T_{n-1,k}) + \Delta T_{n,k} \cdot (1 - 2\ \psi)$$

with:
$$\psi = (\Delta t / \Delta x^2 / (\rho \cdot c_p / \lambda))$$

whereas the left ($x = 0$) boundary condition gave the following by parabolic extrapolation:

$$\Delta T_{1,k+1} = (4 \cdot \Delta T_{2,k+1} - \Delta T_{3,k+1} + 2 \cdot \Delta x \cdot P_0 / \lambda) / 3$$

while the right ($x = \infty$) boundary condition gave the following by parabolic extrapolation: $\Delta T_{N,k+1} = 0$,
with the initial condition: $\Delta T_{n,1} = 0$, $n = 1, 2, \ldots, N$.

Figure 17 shows an example of the curve plots from the aforementioned solution of equation (14) at selected times. A useful value is the heat penetration depth of the medium at t:

$$s_\Theta = \kappa \cdot (\lambda \cdot t / \rho / c_p)^{1/2} \tag{15}$$

which is defined as: $(1/\Delta T(0,t)) \cdot \int \Delta T(x,t) \cdot dx$ (see [7]). The coefficient κ value depends on the form of the boundary condition; which here is $\kappa = 0.9$.

The curve plots in Fig. 17 can be approximated with the following expression to an accuracy level which is sufficient to estimate the results:

$$\Delta T(x,t) = \Delta T(0,t)\cdot\exp\left(-x / s_{\Theta}(t)\right) \tag{16}$$

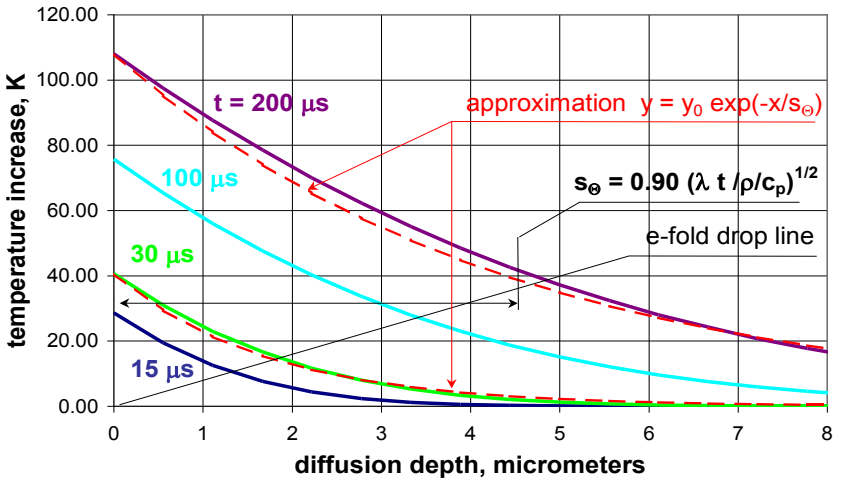

Fig. 17. Heat diffusion into the half space filled with the PM at the pre-set boundary power $P = 5 \times 10^6$ W/m^2 = a constant; $\lambda_{MP} = 0.25$ W/m/K, $\rho_{MP} = 2300$ kg/m^3, $c_{pMP} = 900$ J/kg/K; approximating curves shown

4.2. Pre-set boundary temperature $\Delta T(0,t)$

Heat penetration into the medium can be approximated as described in equation (16); and in the special case: $\Delta T(0,t) \sim (t / \Delta t)^{\alpha}$ (Δt is the heating process end time) – the coefficient κ in formula (15), depending on the exponent α and approximated with the values from Table 4.II [7], expressed with the function:

$$\kappa = 0.564\cdot(\exp(-\alpha/15) + \exp(-\alpha/1.1)) \tag{17}$$

5. POTENTIAL HEAT SOURCES IN A PRIMER CAP INITIATED BY THE FIRING PIN

5.1. Primer cap base indented dome

Given that the energy $E_{Met} \approx 304$ mJ (see Table 4) is fully converted into heat which is homogeneous in a base volume section $V_{met} \approx \pi \cdot r_w^2 \cdot \delta$ at the indentation radius $r_w \approx 1.04$ mm, corresponding to the penetration depth d_z and the density and specific heat of brass: $\rho_m \approx 8500$ kgm^{-3}, $c_{pm} \approx 385$ J/kg/K [6], the temperature of the indentation area will rise by:

$$\Delta T = E_{Met} / (\pi \cdot r_w^2 \cdot \delta \rho_m \cdot c_{pm}) \approx 76 \text{ K}$$

The explosive decomposition temperature of $Hg(CNO)_2$ (which is the primary component of the PM) is $T_{thr} \approx 438$ K (165°C) [3]; the tests were carried out at ambient temperature $T_{env} = 288$ K (15°C), so the temperature rise required for a contact initiation of the reaction should be $\Delta T \geq 150$ K. Hence the primer cap base, which is heated during the deformation, cannot be qualified as the source of initiation.

5.2. Internal heating of the PM at the shearing wave front on the indentation radius

The heat generated on the side surface of the cylinder with radius r_w remains behind the front of the displaced cylindrical surface. Given (as an assumption) that the displaced cylindrical surface is a wave that propagates radially through the PM outside the internal cone, an assumption can be made that up to $r_w(d_z) \approx 1.04$ mm, the wave uniformly heats the volume $V_{PMo} \approx \pi (r_w^2 \delta_{PM} - r_K^3 / 3)$. The energy output $E_{PMo} \approx 24.5$ mJ (see Table 4) at the PM density and specific heat: $\rho_{PM} = 2300$ kgm^{-3}, $c_{pPM} = 900$ J/kg/K [3], when fully converted into heat, heats the volume by:

$$\Delta T = E_{PMo} / (\pi \cdot (r_w^2 \delta_{PM} - r_K^3 / 3) \cdot \rho_{PM} \cdot c_{pPM}) \approx 5.7 \text{ K}$$

Although this effect is negligible.

5.3. Heating on the PM internal cone surface (Fig. 4)

The energy input $E_{PMi} \approx 14.7$ mJ (see Table 4) was assumed to be converted into heat by friction on the SW surface ("Σ") and dissipated by diffusion in a direction perpendicular to the SW surface and on both its sides to depth s_Θ (15), i.e. to the inside of the SW and to the LPM which flows around the cone (Figs. 4 and 18).

It was assumed that one half of E_{PMi} was entrained with the LPM, while the other half was accumulated at the subsurface layer inside the SW, at its base (within ring "4" highlighted in red in Fig. 4). Example: if τ_F = 1 ms, λ_{PM} = 0.25 W/m/K, ρ_{PM} and c_{pPM} is as above, $s_\Theta = \kappa\,(\lambda_{PM} \cdot \tau_F / \rho_{PM} / c_{pPM})^{1/2} \approx 9.89$ μm.

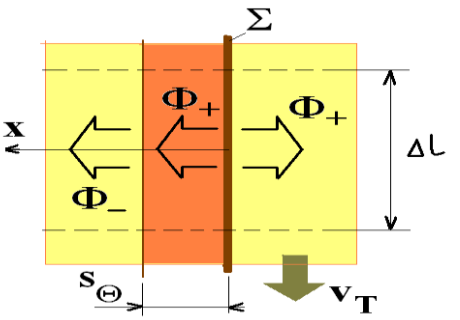

Fig. 18. Diagram of heating a section of the initiation hot spot ("4" in Fig. 4):
Σ – PM shearing and heat output surface;
s_Θ – heated layer (thermal skin); see text for details

Given that the heat output is homogeneous across the entire SW surface (and homogeneous at depth s_Θ) – which would be a gross overestimation, because what is critical is the part of that surface contained between the primer cap base underside surface and anvil, and the same part is decreasing over time – the heated volume was $V_{PMi} \approx \pi\, r_K^2\, s_\Theta$. The temperature gain in the volume defined as above was:

$$\Delta T = E_{MPi} / (\pi \cdot r_K^2 \cdot s_\Theta \cdot \rho_{MP} \cdot c_{pMP}) / 2 \approx 458\ \mathrm{K} > T_{thr} - T_{env}$$

Hence the site (red ring "4" in Fig. 4) is the initiation hot spot (HS).

6. THERMAL CONDITIONS OF CRITICAL VELOCITY AND CRITICAL ENERGY

It was assumed that the energy output in the form of heat generated by friction per **unit of time and slip surface area Σ** (Fig. 18, and "3" in Fig. 4), which is the friction power per unit of surface area is $R_{PM} \cdot v_T$ (unit energy $E_J = \int R_{PM} \cdot dl = \int R_{PM} \cdot v_T \cdot dt$; hence $P_J = dE_J/dt = R_{PM} \cdot v_T$, dl – the SW generating line length differential). An assumption was made similar to that in Section 5.3 that energy is dissipated in either direction from the surface Σ (and input to the HS as a heat flux Φ_+) with the power per surface area unit:

$$P = R_{PM} \cdot v_T / 2 = \Phi_+$$

Let us investigate the heating of an element with $\Delta\ell << \delta_{PM}$ of the hot spot (HS). The modulus (power per surface area unit) of the heat flux output from the subsurface layer into the SW is:

$$\Phi_{-} = \lambda_{PM} \cdot |d\Delta T/dx|$$

with the SW internal surface gradient is, according to formula (16):

$$d\Delta T/dx\ (x=0) = -\Delta T(0,t) / s_{\Theta}$$

The critical case occurs when the power P or the velocity v_{igl} become insufficient to ensure the correct temperature gain of the HS in time. **Temperature gain cessation** is $\Phi_{-} = \Phi_{+}$; hence:

$$\lambda_{PM} \cdot \Delta T(0,t) / s_{\Theta} = R_{PM} \cdot v_T / 2 \qquad (18)$$

Further considerations were based on the aforementioned calculation results (see Section 3.3, Figs. 6 to 11). It was assumed that the firing pin velocity decreases linearly from v_{igl} at $t = 0$ to zero at τ_F over distance d_z (this premise still allowed some freedom from an overt dependence on time).

Hence: $$\tau_F = 2 \cdot d_z / v_{igl} \qquad (19)$$

and: $$v = v_{igl} \cdot (1 - v_{igl} \cdot t / 2 / d_z) \qquad (20)$$

therefore: $$x_i = v_{igl} \cdot t \cdot (1 - v_{igl} \cdot t / 4 / d_z) \qquad (21)$$

$$t_0 = \tau_F \cdot (1 - (1 - (\delta_{PM} - r_K) / d_z)^{1/2}) \text{ with } x_i = \delta_{PM} - r_K = x_{i0} \qquad (22)$$

and: $$\Delta T(0,t) \cdot (\lambda_{PM} \cdot \rho_{PM} \cdot c_{pPM})^{1/2} / \kappa / t^{1/2} = R_{PM} \cdot v_T / 2 \qquad (23)$$

Given that the key values change during the penetration by the firing pin, which lasts $\tau_F = 2 \cdot d_z / v_{igl}$ (19), both sides of the equation (18) must be averaged after this period. Hence, and given that when $v_{igl} = v_{igl(kryt)}$ the HS surface temperature increases by $\Delta T(0,t)$, so the equation for $v_{igl(kryt)}$ is:

$$2 \cdot \Delta T(0,t) \cdot (\lambda_{PM} \cdot \rho_{PM} \cdot c_{pPM})^{1/2} \cdot (2 \cdot d_z / v_{igl(kryt)})^{1/2} / \kappa = (R_{PM} / 2) [\int_0^{t0} v_{T1} \cdot dt + \int_{t0}^{2\,dz\,/\,vigl(kryt)} v_{T2} \cdot dt] \qquad (24)$$

where v, t_0, v_{T1}, v_{T2}, and s_{Θ} are defined with (20), (22), (7b), (10b), and (15), respectively.

When a new integration variable is introduced, $\varepsilon = v_{igl} \cdot t / 2 / d_z$, the equation (24) can be rewritten into:

$$2 \cdot \Delta T(0,t) \cdot (\lambda_{PM} \cdot \rho_{PM} \cdot c_{pPM})^{1/2} \cdot (2 \cdot d_z / v_{igl(kryt)})^{1/2} / \kappa = R_{PM} \cdot 2^{1/2} \cdot d_z \cdot C_1$$

$$\text{with: } C_1 = {}_0\int^{\varepsilon^*} (1-\varepsilon)\cdot r_{wn}(\varepsilon)\cdot \mathrm{d}\varepsilon + {}_{\varepsilon^*}\int^{1} \{(1-\varepsilon)\cdot (r_{wn}(\varepsilon))^2 / [(r_{wn}(\varepsilon))^2 - 1]\}\cdot \mathrm{d}\varepsilon$$

$$r_{wn}(\varepsilon) = [(r_i / r_K)^2 - (r_i / r_K - (2\cdot d_z / r_K)\cdot\varepsilon\cdot(1-\varepsilon/2)^2]^{1/2}$$

$$\varepsilon^* = 1 - (1 - (\delta_{PM} - r_K) / d_z)^{1/2},$$

and transformed further into:

$$4\cdot(\Delta T(0,t) / \kappa)^2 \cdot (\lambda_{PM}\cdot\rho_{PM}\cdot c_{pPM}) / R_{PM} = R_{PM}\cdot v_{igl(kryt)}\cdot d_z \cdot C_1^{\,2} \qquad (25)$$

The expression $R_{PM}\cdot d_z$ is the energy output from the firing pin for the entire distance of penetration of the primer cap, i.e. the work per unit area of the SW shearing surface.

The same work on the SW lateral surface, $S_{con} = 2^{1/2}\cdot\pi\cdot r_K^{\,2}$, should be $R_{PM}\cdot S_{con}\cdot d_z \approx E_{PMi}$. Table 4 indicates that E_{PMi} is a constant component of the available initial energy E_{we}: mean $\eta = E_{Mpi} / E_{we} = 0.0429$. Hence, $R_{PM}\cdot d_z \approx \eta\cdot E_{we} / S_{con}$ and (25) can be rewritten into:

$$4\cdot(\Delta T(0,t) / \kappa)^2 \cdot (\lambda_{MP}\cdot\rho_{MP}\cdot c_{pMP}) / R_{MP} = \eta\cdot(E_{we} / S_{con})\cdot v_{igl(kryt)}\cdot C_1^{\,2}$$

If d_z = 0.554 mm (see Table 4) and all applicable values as above, the following results for KWM-3 at $\Delta T(0,t)$ = 150 K (equivalent to the $Hg(CNO)_2$ initiation temperature [3]):

$$E_{we}\times v_{igl(kryt)} \approx 4\cdot S_{con}\cdot(\Delta T(0,t)/\kappa)^2\cdot(\lambda_{PM}\cdot\rho_{PM}\cdot c_{pPM})/(R_{PM}\cdot\eta\cdot C_1^{\,2}) = 0.176 \qquad (26)$$

The resulting value of $E_{we}\times v_{igl(kryt)}$ is only approximately 30% higher than the value expressed in formula (1). This result is quite acceptable, given the number of simplifications. Hence the $v_{igl(kryt)}$ value can be equated with $v_{i50\%}$ at E_{we} = const. Given the results from Tables 2 and 3 and that E_{we} and $v_{igl(kryt)}$ are equivalent in the expression (26), both values will become critical when they meet formulas (1) or (26) due to the heat removal from the reaction hot spot.

7. OTHER POTENTIAL PM INITIATION MECHANISMS

The following presents a consideration of other potential initiation mechanisms, which are as hypothetical as the internal friction mechanism discussed in Section 3.2.

7.1. Percussion cap initiation type

At the end of indenting the primer cap with the firing pin, most of the PM has already been crushed between the primer cap base, which is subject to indentation (in the shape of a ball with r_i), and the anvil; between those two barriers a layer of PM resides the thickness of which is $x^* = \delta_{PM} - x_i << 2\ r_K$, with a Young's modulus of $Y \approx 10$ GPa.

The surface area of this residual PM layer is limited by the diameter at which the residual layer thickness is increased to $2\,x^*$. When $x^* \approx 0.2\,r_K$, the said diameter is $2\,r_K$, when $x^* \approx 0.1\,r_K$, the diameter is approx. $1.4\,r_K$, and when $x^* \approx 0.05\,r_K$, it is r_K; hence the diameter of this "percussion cap" formed by the residual layer is $S_{kap} = \xi \cdot \pi \cdot r_K^2$, with, respectively, $\xi \approx 1$, 0.5 and 0.25. Given that the anvil remains stationary, the residual PM layer cannot (or can, albeit with a very low probability) be subject to further crushing out to the sides. It can only be compressed further by reducing its thickness by Δx^*.

The compression force was assumed to be expressed as: $F = S_{kap} \cdot Y \cdot \Delta x^*/x^*$, whereas the accumulated deformation energy, $E_s \approx S_{kap} \cdot Y \cdot x^* \cdot (\Delta x^*/x^*)^2/2$, is converted into heat from its entire volume (the conversion is homogeneous).

The anvil is supported by brass brackets the total cross-sectional surface area of which is approx. $2S_{kap}$; hence compression can occur up to $F = 2 \cdot S_{kap} \cdot R_m$, which, given the Y, r_K as above and $R_m = 300$ MPa gives the maximum value of $\Delta x^*/x^* \approx 0.06$. The compression energy thus restricted would reach $x^* = 100$ μm, $E_s \approx 1.4$ mJ at its maximum.

The energy balance:

$$E_s \approx S_{kap} \cdot x^* \cdot Y \cdot (\Delta x^* / x^*)^2 / 2 = \Delta T \cdot \rho_{MP} \cdot c_{pMP} \cdot S_{kap} \cdot x^*$$

would, under these conditions and with the aforementioned constant values, result in a temperature gain of the said percussion cap of $\Delta T = Y \cdot (\Delta x^* / x^*)^2 / (2 \cdot \rho_{PM} \cdot c_{pPM}) \approx 8.7$ K, which would definitely be far too small to initiate the primer cap. This type of initiation might be possible with a different design solution.

7.2. Crystal breakup

The crystals forming the PM could crack and fracture under external loads. A single fracture process breaks the chemical bonds of a crystal. On the one hand, free radicals may form, or the (sensitive) crystal may lose its metastable equilibrium and trigger a chemical reaction; on the other hand, the fracture may leave uncompensated heteropolar electrical charges on the fracture surfaces, where a substitute diameter d_{crack} describes the child crystals [8]. Given that the surfaces of a fracture break away from each other in time and remain parallel to each other, they can be viewed as the electrodes of a diode the capacity of which is $C = \varepsilon_0 \cdot \pi \cdot d_{crack}^2 / 4 / w$, where ε_0 – vacuum dielectric permittivity, w – electrode surface spacing. If the electric force $E = u/w$ is high enough (u – electrode to electrode voltage), as generated by the uncompensated charges, this diode may go into a cold emission state with a current density of:

$$j = 1.55 \times 10^{-6} \cdot (E^2/W) \exp(-6.9 \times 10^7 \cdot W^{3/2} / E)$$

(j in [A/cm^2], W – in [eV], E – in [V/cm]) [9] – where the electrons may be ripped away from one of the surfaces, collide with the molecules on the other surface and trigger a decomposition reaction, provided that the energy $e \times u$, acquired by an electron in the electric field (e – electron charge), is noticeably (or significantly) higher than the work of the electron output W from the crystal. Given that $E \approx q /(2 \cdot \pi \cdot \varepsilon_0 \cdot d_{crack} \cdot r_{edge})$ and an emission surface area $S_{ems} \approx 2 \cdot \pi^2 \cdot d_{crack} \cdot r_{edge}$, with r_{edge} – the radius of rounding of the fracture edge, an equation was solved for the conservation of the electric charge, $q = C \cdot u$: $dq/dt = S_{ems} \cdot j$, where $W = 3.5$ eV, $d_{crack} = 2$ μm with the fracture surface separation velocity $v_{fragm} = 3$ m/s.

Fig. 19 shows the results for the initial charge of $q_0 = 10^{-14}$ C (coulombs). As we can see, just 2 ns after the fracture, a process of electron generation begins where the electron energy is > 5 eV with the count of ~ 10/ fs = 10^4/ ns at $E \approx 2.5$ GV/m and a gap of ~ 5 nm. The electrons may be generated in a vacuum, with the air filling the void at the speed of sound (minus the viscosity) in < 3 ns. The "diode" hence ceases to function.

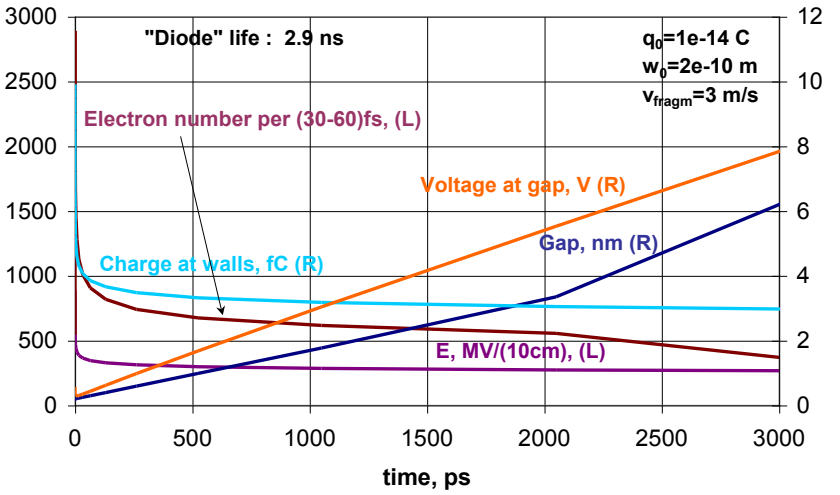

Fig. 19. Parameters of cold emission for a diode formed by a fracturing crystal; (*L*) and (*R*) – affiliation of the curve to, respectively, the left-hand or the right-hand scale of the ordinate axis.

The assumption of $q_0 = 10^{-14}$ C is too optimistic; as measured in [8], after 1 ms, the surface density values of the electric charge on the crystal fracture surfaces were 0.3÷1 μC/m^2; given $d_{crack} = 2$ μm, the result would be $q_0 = 10^{-18}$ C, and the calculations gave the result $E < 9$ kV/m in the same conditions, meaning that no cold emission of electrons occurs.

The incidents of fracture may occur already at the beginning of the firing pin penetration process, which would result in irregular time delay values of the primer cap initiation, especially in the function of v_{igl} (see Fig. 15). The fracture incidents may occur already during the manufacturing pressing of the PM shape; however, the PM is not initiated at that time. Once fractured, the pieces of a crystal require room to depart from each other and form their own electrode gap. This is highly unlikely in a highly compressed pyrotechnic mixture. Given the foregoing, this mechanism must be rejected from the investigation.

7.3. Ambient heating by compressed intercrystalline gas during the crushing of PM

Assuming that adiabatic compression is applied with the exponent of $\gamma = 1.4$, and preserved symmetry of compression to a spherical gas bubble the mass of which is m_g, the initial pressure is p_{g0} and the diameter is d_0 (while the corresponding current values are p_g and d). The gas density is expressed as $\rho = 6 \cdot m_g/\pi/d^3$; the gas volume is $V = m_g/\rho$; the equation of state is $p_g = p_{g0} \cdot (\rho/\rho_0)^\gamma = p_{g0} \cdot (d_0/d)^{3\gamma}$; and the energy input to the gas bubble compressed from the diameter d_0 to d_1 is:

$$\Delta E_g = \int_{d0}^{d1} p_g \cdot \mathrm{d}V = (\pi \cdot p_{g0} \cdot d_0^{\,3}/6 \,/\, (\gamma - 1)) \cdot ((d_0/d_1)^{3(\gamma - 1)} - 1)$$

Assuming that this model can approximate the compression of gas (i.e. air) within the pores between the PM crystals, then the initial size of the pores (at the bulk density) reach the size of the crystals themselves (2÷10 μm). However, in its manufacturing process, the PM is highly compressed into a shape the density of which is near the density of a homogeneous material. If the pores occupy 1% of the finished PM shape volume, the mean pore size, equivalent to d_0 of the gas bubble, is 0.4÷2 μm. If the compressive forming of a PM shape is long enough, the air will escape from between the crystals and $p_{g0} \approx 100$ kPa (ambient pressure). Given that the compression from $d_0 = 2$ μm is in effect until the gas reaches the density of the surrounding solid, i.e. $p_{g0} \approx 100$ kPa, and with a large surplus of $d_0/d_1 \approx 26$, the resulting energy is $\Delta E_g = 5.14 \times 10^{-11}$ J. This is enough energy to heat up the air in a thermally insulated gas bubble by $\Delta T = 10^4$K. If the gas bubble wall convergence velocity is similar to the firing pin indentation velocity (Figs. 6-9): $v_g \approx v_{g0} \cdot (1 - t/\tau_F)$, $v_{g0} \approx 2 \cdot d_0 / \tau_F$, the energy within the gas bubble increases in time:

$$\Delta E_g = (\pi \cdot p_{g0} \cdot d_0^{\,3} / 6/(\gamma - 1)) \cdot (1 / (1 - (v_{g0} \cdot \mathrm{t} / 2 / d_0)^2)^{3(\gamma - 1)} - 1)$$

If we assume that the heat generated in this manner inside the gas bubble does not **diffusively** heat the gas but (for the sake of simplicity) **only** the PM ambience the volume of which is $(4\pi/3)\ s_\Theta^3$, and assuming that the diffused energy is equal to ΔE_g, the temperature increases in time within a thermal skin of thickness s_Θ around the gas bubble:

$$\Delta T\,(t) = [p_{g0}\cdot d_0^{\,3}\cdot(\rho\cdot c_p)^{1/2}/8/\kappa^3/(\gamma-1)]\cdot[1/(1-(v_{g0}\cdot t/2/d_0)^2)^{3(\gamma-1)}-1]/\lambda\cdot t)^{3/2} \quad (27)$$

Figure 20 shows two examples of tabulating the formula (27) up to time $\tau_F \approx 500$ μs (a representative value for the typical operating conditions of the investigated primer caps) – when $d_0/d_1 \approx 26$ is achieved at $\lambda = 0.25$ W/m/K, $\rho = 2\ 300$ kg/m^3, $c_p = 900$ J/kg/K, p_0, d_0, γ – as above, for the coefficient κ determined with the formula (17) for the selected coefficient value of $\alpha = 0.85$-1.4, which ensures a progression $(t\ /\ \Delta t)^\alpha$ similar to that of (27) (a higher value of α gave an approximate derivative at the end of the curve).

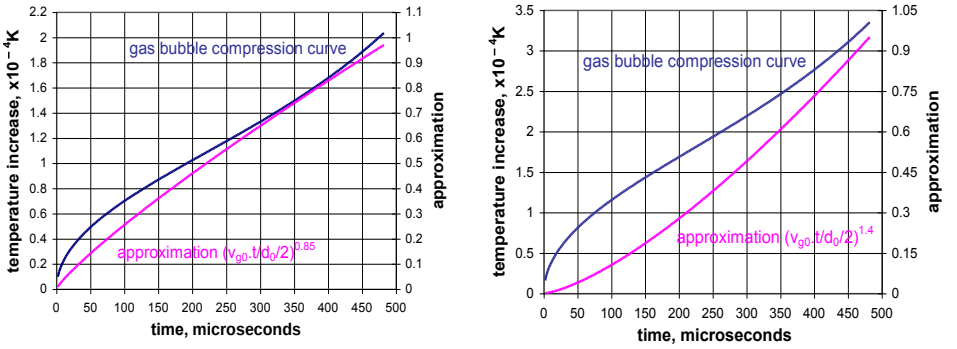

(a) (b)

Fig. 20. Approximation of the compression curve for a gas bubble in time with a function $(t\ /\ \Delta t)^\alpha$ (see Section 5.2): a) $\alpha = 0.85$, b) $\alpha = 1.4$

The PM temperature gains were negligible in both α cases. Anyhow, actual gas bubbles within an PM shape usually retain forms very different from spherical symmetry; when the gas bubbles are compressed, the gas bubbles escape into the gaps between the (deformed) crystals, and a state of instability begins to evolve which makes further compression difficult. Hence this mechanism cannot be qualified as contributory to the primer cap initiation problem presented here.

8. CONCLUSIONS

It was experimentally proven that when the percussion striker energy is constant at E_{we} = 272 mJ or 343 mJ, decreasing the firing pin velocity v_{igl} (and increasing the striker mass) reduced the initiation probability $p(v_{igl})$ of the KWM-3 primer cap. The v_{igl} value at which $p(v_{igl})$ was reduced to 0.5 is $v_{i50\%} \approx 0.34 \div 0.51$ m/s.

Experimental data suggest that the product $E_{we} \times v_{i50\%}$ might be a constant, the value of which was approx. 0.136 for the tested primer caps.

The few (due to technical constraints) results from a different type of testing with variable E_{we}, $p(E_{we50\%}) = 0.5$, provided $E_{we50\%} \times v_{igl} \approx 0.16 \div 0.19$, which is fairly close to the previous energy value. The values can be determined by further investigation.

The work suggests that a pair of critical initiation parameters exists, $E_{we50\%}$ and $v_{i50\%}$, coupled by a numeric constant specific to primer cap type.

A model was presented for the indentation/penetration of the primer cap with the firing pin; however, it was only a first approximation of the solution to the investigated problem and requires further research into the deformation of primer cap bases and the pyrotechnical mixtures of the cap. Despite its simplicity, the model allowed a visualisation of the temporal progression of the indentation (penetration) depth and velocity, the forces of resistance from primer cap components, the energy output in the components, and the energy output power. The model contemplated here assumed **that the entire energy of the percussion striker was transferred to the primer cap** (by perfect non-elastic impact). The firing pin penetration times determined with the model for various percussion striker masses (i.e. velocity v_{igl} values) were very close to the primer cap initiation delay times measured with the same striker masses (approx. 0.5÷6 ms, see Table 5), which indirectly and positively verified the assumption of a (nearly) non-elastic impact mechanism.

It was assumed that the primer cap was initiated by thermal conversion of the friction (shearing) energy over a specific conventional surface Σ inside the pyrotechnic mixture shape; the energy (E_{PMi}) output from E_{we} had an efficiency of approx. 4%, as calculated with the aforementioned model. It was demonstrated that this energy volume was enough to heat up the thermal diffusion skin layer of Σ to a temperature which greatly exceeded the explosive decomposition temperature of $Hg(CNO)_2$ (the main component of the PM).

The observed reduction of $p(v_{igl})$, concomitant to the reduction of v_{igl} at E_{we} = const was assumed to be related to the balance between the power P_{PMi} of E_{PMi} input to a potential ignition hot spot on Σ and the heat flux Φ_ dissipated from the same hot spot into the remaining volume of the pyrotechnic mixture.

Given $\Phi\_ = P_{PMi}$ at the ignition temperature of $Hg(CNO)_2$, the calculation results from the aforementioned model were used to produce the expression $E_{we} \times v_{i50\%} \approx 0.18$. Here the constant approximated the values obtained from the experiments, which partially validated the model.

The mean power of primer cap base indentation, corresponding to $v_{i50\%} \approx 0.34 \div 0.51$ m/s, was $P_{avg50\%} = 120 \div 180$ W, and its maximum was $P_{max50\%} = 170 \div 250$ W (see Fig. 15).

Hence it was demonstrated that not only is the energy important in the process of percussive initiation, but also the power of energy transmission as it relates to the velocity of the percussion striker/firing pin.

The technical constraints of this work have not permitted the authors to detect any sharp threshold in the decline in initiation below $v_{i50\%}$.

The broadening of such a threshold might result from a statistical scatter of the mechanical and chemical parameters of the manufacturing process (i.e. the non-homogeneity of the PM chemical composition at low volumes may cause an inconsistent explosive decomposition of $Hg(CNO)_2$ microcrystals at a given temperature, depending on the neighbouring crystal admixture).

Further investigation is required into the relationship between E_{we} and the energy actually absorbed by the primer cap subject to deformation.

In this discussion it was stated that other mechanisms, as offered in the references, i.e. adiabatic heating of gases in the intercrystalline pores of the pyrotechnical mixtures, PM crystal cracking (fracture), or the "percussion cap" effect cannot satisfactorily explain the initiation of the primer caps. What does explain this initiation is the friction occurring on the fracture/slide surfaces within the pyrotechnical mixture shape. A diagram of this proposed mechanism is shown in [3] and Section 3.

REFERENCES

[1] Dębiński Jarosław, Andrzej Długołęcki, Andrzej Faryński, Edward Olejniczak, Andrzej Żyluk. 2013. „Pomiary parametrów spłonek uderzeniowych". *Problemy mechatroniki. Uzbrojenie, lotnictwo, inżynieria bezpieczeństwa – Problems of Mechatronics. Armament, Aviation, Safety Technology* 4 (2) : 43-52.

[2] Bielajew Mikołaj Michajłowicz, 1956. *Wytrzymałość materiałów*, Warszawa: Wydawnictwo MON.

[3] Dębiński Jarosław, Andrzej Długołęcki, Andrzej Faryński. 2013. „Model numeryczny uderzeniowego pobudzenia spłonki w urządzeniu testowym ITWL". *Problemy mechatroniki. Uzbrojenie, lotnictwo, inżynieria bezpieczeństwa – Problems of Mechatronics. Armament, Aviation, Safety Technology* 4 (4) : 41-52.

[4] SWW 1333 marketing brochure published by "MESKO".

[5] Janus Elżbieta (ed.). 1981. *Poradnik warsztatowca-mechanika*. Warszawa: WNT.
[6] Mizerski Witold, (ed.). 2002. *Tablice fizyczno-astronomiczne*. Warszawa: Adamantan.
[7] Knoepfel Heinz, 1972. *Sverkhsilnye impulsnye magnitnye polya* (Russian language). Moskva: Mir. (see also *Pulsed High Magnetic Fields*, North Holland, Amsterdam-London 1970).
[8] Faryński Andrzej, Roman Kamiński, Zbigniew Ziółkowski, 2004. Elektryzacja drobin piasku w procesie ich mechanicznego kruszenia. *EL-TEX 2004 – VI Międzynarodowe sympozjum „Pola elektrostatyczne i elektromagnetyczne – nowe materiały i technologie"*. Łódź. 25–26 November 2004.
[9] Winterberg Friedwardt, 1974. Poluchenye plotnoi termojadernoi plazmy pri pomoshchi intensivnykh relativistskikh elektronnykh puchkov. W *Fizika vysokikh plotnostei energii* (Russian language). ed. P. Caldirola & H. Knoepfel. Moskva: Ed. Mir.

Wyznaczanie krytycznej prędkości iglicy i mocy krytycznej przy uderzeniowym pobudzaniu spłonki

Andrzej FARYŃSKI, Andrzej DŁUGOŁĘCKI, Jarosław DĘBIŃSKI, Łukasz SŁONKIEWICZ

Streszczenie. W pracy przeprowadzono badania prawdopodobieństwa pobudzenia spłonki typu KWM-3 w funkcji prędkości uderzającej iglicy. Prędkość nadawała iglicy spadająca masa. Pomiary prowadzono za pomocą układu i metod opracowanych w ITWL. Prędkość i moc impulsu uderzeniowego zmieniano poprzez zmianę masy uderzeniowej tak, aby zachować stałość energii impulsu inicjującego na dwóch poziomach: E_{we} = 272 mJ i 343 mJ. Oszacowane na podstawie danych doświadczalnych prędkości iglicy, dla których występuje 50% prawdopodobieństwo pobudzenia mieszczą się w przedziale $v_{i50\%}$ = 0,34÷0,51 m/s. Stwierdzono, że średnia zwłoka czasowa zadziałania spłonki rosła od ok. 0,7 ms przy prędkości uderzenia wynoszącej 1,5 m/s do 6 ms przy 0,17 m/s. Dane doświadczalne sugerują $E_{we} \times v_{i50\%} \approx 0{,}136$. Zaproponowano uproszczony model deformacji dna spłonki i sprasowanej kształtki mieszaniny pirotechnicznej, za pomocą którego przy założeniu całkowitego przekazania energii spłonce przez masę uderzeniową wyznaczono w sposób przybliżony przebiegi w czasie zagłębiania iglicy w spłonkę i jego prędkości, mocy i wydzielanej energii. Obliczona na podstawie modelu średnia moc w czasie impulsu inicjującego dla podanych $v_{i50\%}$ wynosi odpowiednio P_{avg} = 120÷180 W, natomiast moc maksymalna P_{max} = 170÷250 W. Otrzymane w wyniku obliczeń czasy zagłębiania iglicy są bardzo bliskie wyżej wymienionym czasom zadziałania spłonek dla odpowiednich prędkości i mas uderzeniowych, co pośrednio świadczy o niemal całkowitym przekazaniu przez te masy energii spłonkom. Wskazano miejsce w kształtce mieszaniny pirotechnicznej, które może być ogniskiem inicjowania reakcji wybuchu. Na podstawie wyników obliczeń opartych o ten model, przyjmując równość mocy doprowadzania energii i dyfuzyjnego odprowadzenia strumienia ciepła do i z ogniska w temperaturze inicjacji, wyprowadzono wyrażenie na $E_{we} \times v_{i50\%}$, które dało wartość ok. 0,18. Świadczy to o tym, że dwa parametry krytyczne pobudzenia spłonki – prędkość, którą można utożsamić z $v_{i50\%}$ (i odpowiednia moc) oraz $E_{we50\%}$ – energia, poniżej której prawdopodobieństwo pobudzenia spłonki spada poniżej 0,5, są związane ze sobą. Oprócz mechanizmu pobudzenia zaproponowanego i użytego do obliczenia prędkości krytycznej dyskutowano inne mechanizmy, które wykluczono.

Słowa kluczowe: uderzeniowa inicjacja spłonki, moc krytyczna, zwłoka czasowa, prawdopodobieństwo zapłonu